Evolutionarily conserved function of the *even-skipped* ortholog in insects revealed by gene knock-out analyses in *Gryllus bimaculatus*

Yuki Nakamura

Department of Biological Science and Technology

College of Life and Material Systems Engineering

Graduate School of Advanced Technology and Science

Tokushima University

September 2022

Contents

1. Abstract

Comparing the developmental mechanisms of segmentation among insects with different modes of embryogenesis provides insights on how the function of segmentation genes evolved. Functional analysis of *eve* by genetic mutants shows that the *Drosophila* pair-rule gene, *even-skipped* (*eve*), contributes to initial segmental patterning. However, *eve* orthologs tends to have diverse functions in other insects. To compare the evolutionary functional divergence of this gene, I evaluated *eve* function in a phylogenetically basal insect, the cricket *Gryllus bimaculatus*. To investigate the phenotypic effects of *eve* gene knock-out, I generated CRISPR/Cas9 system-mediated mutant strains of the cricket. CRISPR/Cas9 mutagenesis of multiple independent sites in the *eve* coding region revealed that *eve* null mutant embryos were defective in forming the gnathal, thoracic, and abdominal segments, consequently shortening the anterior-posterior axis. In contrast, the structures of the anterior and posterior ends (e.g., antenna, labrum, and cercus) formed normally. Hox gene expression in the gnathal, thoracic, and abdominal segments was detected in the mutant embryos. Overall, this study showed that *Gryllus eve* plays an important role in embryonic elongation and the formation of segmental boundaries in the gnathal to abdominal region of crickets. In the light of studies on other species, the *eve* function shown in *Gryllus* might be ancestral in insects.

2. General Introduction

2.1. Evolution in segmental structures of arthropod

Segmental structures are major factor of the body plan in arthropoda, which has the most abundant taxon among animalia. The segmental structures of the arthropod are diversified among major taxa. For example, a pair of arthropod appendages are in principle formed on each segment; however, they have evolved into various forms for different purposes (e.g. walking, flying, and capturing food), depending on the taxon and the body region where the appendages are formed. Furthermore, millipede *Diplopoda* seemingly appears to have two pairs of legs on one segment of the trunk region because almost all trunk segments coalesce together in two of each segment. Therefore, the segmental structures are an extremely important feature in considering the evolution of arthropod forms.

Segmentation genes and mechanism have been revealed using a model animal; fruit fly *Drosophila melanogaster* (Nüsslein-Volhard et al., 1987; Nüsslein-Volhard and Wieschaus, 1980). The segments of *Drosophila* are formed by the mechanism that genes encoding transcription factors hierarchically regulate downstream target genes (Akam, 1987). Owing to these studies, I can compare with the segmentation genes and mechanism in *Drosophila* when studying these in other arthropods, and I can consider how the segmentation process has evolved in the arthropods. Thus, clarifying the genetic background in the segmental structures leads to an understanding of the evolution.

In previous studies, the functions of the segmentation genes in other arthropods have been analyzed mainly by RNA interference. In principle, however, this analysis cannot produce a phenotype of complete loss-of-function. Thus, it is important to analyze the segmentation genes in other arthropods by the gene knock-out.

2.2. The cricket, *Gryllus bimaculatus*, is a valuable model organism

Two-spotted cricket *Gryllus bimaculatus*, which inhabits the tropical and subtropical regions of Asia, Africa, and Europe, can be easily bred in the laboratory. Furthermore, this insect has been widely used to study insect morphology and physiology (Horch et al., 2017). Moreover, since I have been able to use database of its genome sequence (Ylla et al., 2021), it is possible to perform genome editing using *Gryllus* (Watanabe et al., 2012).

Recently, the gene knock-out using clustered regularly interspaced short palindromic repeats (CRISPR)/ CRISPR associated proteins 9 (Cas9) has been able to adapt for *Gryllus*. The CRISPR/Cas9 system is based on a bacterial immune system (Cong et al., 2013; Mali et al., 2013), and RNA-guided DNA endonuclease (Cas9 protein) works binding short RNA fragment (guide RNA) which is used as “guides” to recognize a DNA target sequence. Double-strand breaks (DSBs) introduced by this system can be restored via cellular DNA repair pathways, such as non-homologous end-joining mechanisms. Finally, small insertions and/or deletions are produced at the repair junction, thereby generating mutations. In the case that frameshifts are caused by the mutations, targeted gene knock-out is achieved. As a practical application example, a cricket strain knocking out *Gryllus* dopamine receptor 1 gene is generated, and the knock-out crickets are used for the study of learning and memory (Awata et al., 2015). Therefore, the genome editing and functional analysis of target genes in *Gryllus* using the CRISPR/Cas9 system are now possible at an individual level.

3. Introduction

Comparing the segmentation mechanisms of insects with different modes of embryogenesis provides insights on how the network of segmentation genes has evolved. Insects are arthropods with a segmented body plan that is constructed from the modular organization of fundamentally similar units arranged serially along an anterior-posterior (AP) axis (Hannibal and Patel, 2013). This fundamental body plan exists across all insects. However, the mode of embryogenesis is generally classified by the initial size of the germ anlage (such as short, intermediate, and long germ embryogenesis), and differs among insect species (Davis and Patel, 2002). All segments are almost simultaneously formed in the fruit fly, *Drosophila*, representing a typical model for long germ insects. In the embryogenesis of *Drosophila*, segmentation genes (Akam, 1987; Nüsslein-Volhard et al., 1987; Nüsslein-Volhard and Wieschaus, 1980) form a hierarchical regulation network, including maternal, gap, pair-rule, and segment-polarity, and homeotic genes (Lawrence, 1992). In contrast, in short and intermediate germ insects (e.g., cricket and grasshopper), anterior segments are initially specified, with posterior segments forming progressively during the process of posterior growth (Davis and Patel, 2002). Because the process of segmentation in these insects clearly differs to that in *Drosophila*, the genetic mechanisms underlying this process in these insects might also differ to that in *Drosophila*.

Comparative analysis of the segmentation mechanisms has progressed for various insects, showing that the function of segmentation genes identified in *Drosophila* are not necessarily conserved in other insects. The *even-skipped* (*eve*) gene is a pair-rule gene in *Drosophila*, and is involved in the alternative segmentation of the gnathal to abdominal region (Macdonald et al., 1986). However, this gene contributes to the formation of all segments in

the gnathal to abdominal region, because null mutants exhibit an asegmental phenotype in this region (Macdonald et al., 1986). The *eve* orthologs of *Tribolium* and *Bombyx* are likely to have similar function as in *Drosophila* (Choe et al., 2006; Macdonald et al., 1986; Nakao, 2015). On the other hand, RNAi against the *eve* gene of *Oncopeltus* causes defects in segmentation of almost the entire body in the most severe case, implying that this ortholog has gap gene-like function differently from *Drosophila* (Liu and Kaufman, 2005). Furthermore, although the *Nasonia eve* ortholog results in a pair-rule like phenotype in the anterior embryo, the phenotype is accompanied by posterior truncation of the embryo, suggesting involvement of *eve* in a different manner from *Drosophila* in the posterior segmentation (Rosenberg et al., 2014).

Gryllus bimaculatus is a phylogenetically basal and intermediate-germ insect, which has an *eve* ortholog that contributes to segmentation from the gnathal to posterior terminal region (Mito et al., 2007). Although loss and fusion of some segments were observed in the RNAi phenotype of *Gryllus bimaculatus eve* (*Gb'eve*) ortholog, I was unable to clearly identify the extent of the body segments to which this gene functions (Mito et al., 2007). This is because, in principle, gene knockdown by RNAi cannot suppress expression of a target gene completely. Thus, it would be essential to produce *Gb'eve* null mutants by the genetic mutation to allow a more precise comparison of *eve* function between insect species.

Here, I report the first analysis of *eve* function using genetic mutation in *Gryllus*. The method for generating gene knock-out strains has been established in this species by using genome editing technologies with two artificial nucleases, ZFNs and TALENs (Watanabe et al., 2012). More recently, CRISPR/Cas9-based genome editing technology has also become

available for targeted analyses on genes (Awata et al., 2015; Horch et al., 2017). In the present study, I produced strains of *eve* knock-out (KO) crickets using the CRISPR/Cas9 system and analyzed the KO phenotypes. The suggested *eve* function in *Gryllus* was compared those in other insects to understand the segmentation mechanism of insects involving *eve* from an evolutionary perspective.

4. Results

4.1. Establishment of gene knock-out strains of *Gryllus even-skipped* ortholog by the CRISPR/Cas9 system

I identified the gene structure of the *Gb'eve* cDNA sequence by searching the *G. bimaculatus* genome database (Ylla et al., 2021). *Gb'eve* gene was composed of five exons and four introns, encoding a homeodomain in the second and third exon and a Groucho interacting domain in the fifth exon (Kobayashi et al., 2001) (Fig. 1A). To generate *Gb'eve* KO strains, I designed four gRNAs, which recognize specific sequences on the first and second exons. I named the gRNAs targeting the first exon "gRNA-1 and gRNA-2", and the gRNAs targeting the second exon "gRNA-3 and gRNA-4" (Fig. 1A). The sequence targeted by the gRNA-4 was included in the homeodomain encoding region. Each gRNA was independently injected into eggs at 2-h after egg laying (AEL), together with Cas9 mRNA.

Next, I performed genotyping of the embryos of the injected generation (G0) by the mutation detection assay. I randomly selected eight G0 embryos from eggs injected with each gRNA for extracting genomic DNA. The embryos with CRISPR/Cas9-induced mutations were detected at the rate of 75, 100, 50, and 13% for the gRNA-1, gRNA-2, gRNA-3, and gRNA-

4 respectively (Fig. 1B; the rates of mutation frequency in Table 1). Since the rate of mutation-induced embryos was lower in the case of using the gRNA-4 than other gRNAs, I co-injected larger amounts of gRNA-4 (and gRNA-1 as the control) and Cas9 mRNA to eggs at 2-h AEL. The rate of mutation frequency increased to 100% and 38% for the gRNA-1 and gRNA-4 sites, respectively (Table 1).

I next evaluated whether these mutations would be transmitted to progeny (G1). The survival rates of fertile G0 adults were 25, 2, 40, and 6% in embryos injected with the gRNA-1, gRNA-2, gRNA-3, and gRNA-4, respectively (Table 2). The survival rates of the fertile G0 adults were 26% and 38% in embryos injected with the larger amounts of the gRNA-1 and gRNA-4, respectively (Table 2). For generating strains of a specific mutation, all fertile G0 adults were crossed with wild type (WT) adults. To specify G0 founders and estimate the germline transmission rate for use of each gRNA, the mutation detection assay was performed using genomic DNA extracted from 25 G1 embryos of each crossed adult pair (Fig. 1B). Germline transmission rates were 31, 50, 50, and 0% in fertile G0 adults injected with the gRNA-1, gRNA-2, gRNA-3, and gRNA-4, respectively (Table 2). The rates increased to 60% and 13% in the cases of injecting the larger amounts of the gRNA-1 and gRNA-4, respectively (Table 2).

After the G1 eggs derived from each G0 founder hatched, I further performed genotyping to identify G1 mutant individuals by the mutation detection assay and detected heterozygous mutant nymphs in each strain (Fig. 1B). Interestingly, all the of identified *Gb'eve* heterozygous mutants were female. Therefore, I hypothesized that the *Gb'eve* gene is present on a sex chromosome. In *Gryllus*, males have only one X chromosome (XO), whereas females have two (XX) (Yoshimura et al., 2006). If the *Gb'eve* gene is on the X chromosome, all of mutant males should be hemizygotes for mutant alleles and may be lethal

before the developmental stage when genotyping was done. To verify this hypothesis, I measured the copy number of the *Gb'eve* gene in the genome of WT female and male crickets using quantitative PCR. The relative quantity of the *Gb'eve* gene in the female genome was two-fold higher than that in the male genome (Fig. 2A). The result indicates that the female has two copies of the *Gb'eve* gene and the male has one copy, corresponding to the expected numbers of X chromosome (Fig. 2B).

Through interbreeding *Gb'eve* heterozygous females and WT males, I isolated potential *Gb'eve* hemizygous mutant embryos, which have a clear morphological phenotype (see the next section) (Fig. 2B). I then analyzed DNA sequences of induced and inherited mutations in the mutants and detected insertion and deletion (indel) mutations resulting in frameshifts in each gRNA targeted site except the gRNA-4 site (Fig. 1C and Fig. 3). Consequently, I established a total of six *Gb'eve* knock-out (KO) strains with specific indel mutations for the gRNA-1 (Fig. 1C; strains (1), (2), and (3)), gRNA-2, gRNA-3, and gRNA-4 (Fig. 3).

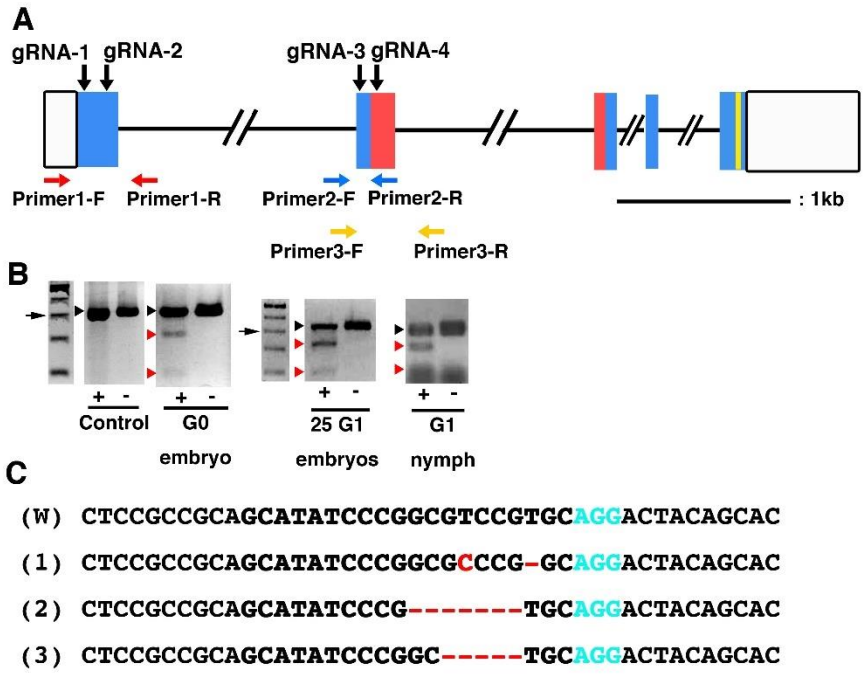

Figure 1. CRISPR/Cas9-induced mutation of the *Gryllus even-skipped* ortholog. (A) Schema of *Gb'eve* gene structure and gRNA targeted sites. The five boxes indicate the five exons, and the black lines indicate the four introns. The regions encoding homeodomain and Groucho interacting domain are presented in red and yellow boxes, respectively. The translated and untranslated regions are presented in blue and white boxes, respectively. gRNA targeted sites are located on the sense or anti-sense strands of exon1 (gRNA-1 and gRNA-2) and the sense strand of exon2 (gRNA-3 and gRNA-4). Primers used in genotyping PCR are indicated in colors colored allows (red, blue, and yellow). Primer 2-F and primer 2-R were used for mutagenesis by the gRNA-3, while Primer 3-F and primer 3-R were used for the gRNA-4. (B) Genotyping of G0 or G1 embryos and G1 nymphs with mutant alleles by the mutation detection assay. The results of assay for the gRNA-1 site are shown as representative ones. Black arrowheads indicate the PCR products for WT alleles. Red arrowheads indicate the PCR products for mutant alleles cleaved by Guide-it resolvase. Arrows indicate 300 bp of sized marker. (C) Sequences of the gRNA-1 site in WT (W) and *Gb'eve* KO (1-3) embryos. The gRNA targeting sequence is presented as a bold black font. The protospacer adjacent motif (PAM) sequence is presented as a blue font. The sequence of deletion mutations and base substitutions is presented as a red font.

Table 1. Rates of mutation frequency in G0 embryos

Targeted sites	Concentration of gRNA and Cas9 mRNA (ng/μl)	Injected embryos	% (no.) mutation frequency[a]
gRNA-1	50/100	61	75(6/8)
	250/500	27	100(8/8)
gRNA-2	50/100	124	100(8/8)
gRNA-3	50/100	38	50(4/8)
gRNA-4	50/100	94	13(1/8)
	250/500	29	38(3/8)
Control[b]	0/100	23	0(0/8)

[a]The mutation frequency rate represents percentage of injected embryos with mutant alleles per selected embryos in the assay.

[b]I injected Cas9 mRNA alone as a negative control.

Table 2. Germline transmission rates.

Targeted site	Concentration of gRNA and Cas9 mRNA (ng/μl)	Injected embryos	% (no.) fertile adults	% (no.) germline transmission[a]
gRNA-1	50/100	61	25(13/53)	31(4/13)
	250/500	27	26(5/19)	60(3/5)
gRNA-2	50/100	124	2(2/116)	50(1/2)
gRNA-3	50/100	38	40(12/30)	50(6/12)
gRNA-4	50/100	94	6(5/86)	0(0/5)
	250/500	29	38(8/21)	13(1/8)

[a]The germline transmission rates represent percentage of G0 founders producing G1 embryos having targeted-site mutations per fertile adults.

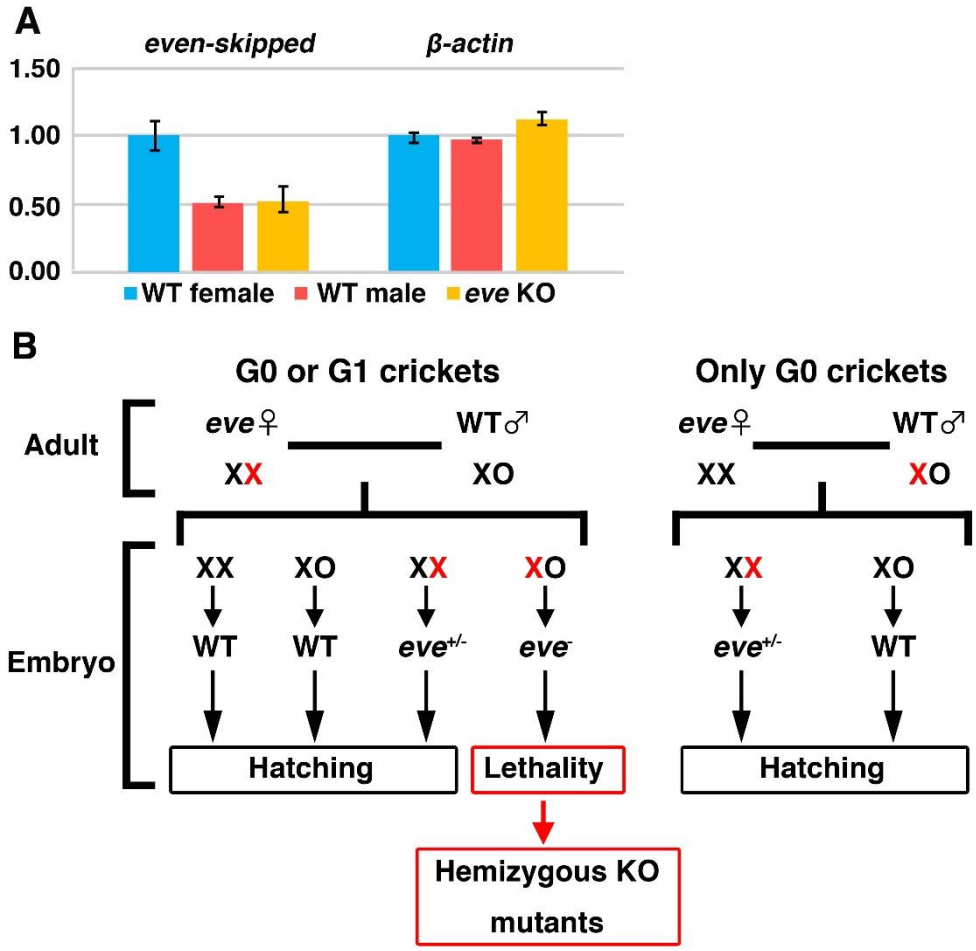

Figure 2. Isolation of *Gb'eve* KO embryos. (A) Measurement of the copy number of *Gb'eve* gene in the genome of female and male crickets by quantitative PCR. The copy numbers of *Gryllus β-actin* gene did not appear to differ in WT female and male crickets. The copy number of *Gb'eve* gene in the genome of a WT female cricket was two-fold higher than that in the genome of a WT male cricket. The copy number of *Gb'eve* gene in the genome of a *Gb'eve* KO embryo was comparable to that in the genome of the WT male cricket. (B) Schema of the inheritance pattern in *Gb'eve*. XX and XO indicating sex chromosome. Normal and mutant alleles are presented in black and red, respectively. Interbreeding G0 or G1 heterozygous adult females with WT adult males, hemizygous KO mutants were obtained. Embryos of WT both sexes and heterozygous female enabled to hatch; however, the hemizygous male embryos did not. Thus, I maintained the heterozygous females as the *Gb'eve* KO strain. In the case of G0, adult males were also used to interbreed with WT adult females, because they tended to be mosaic.

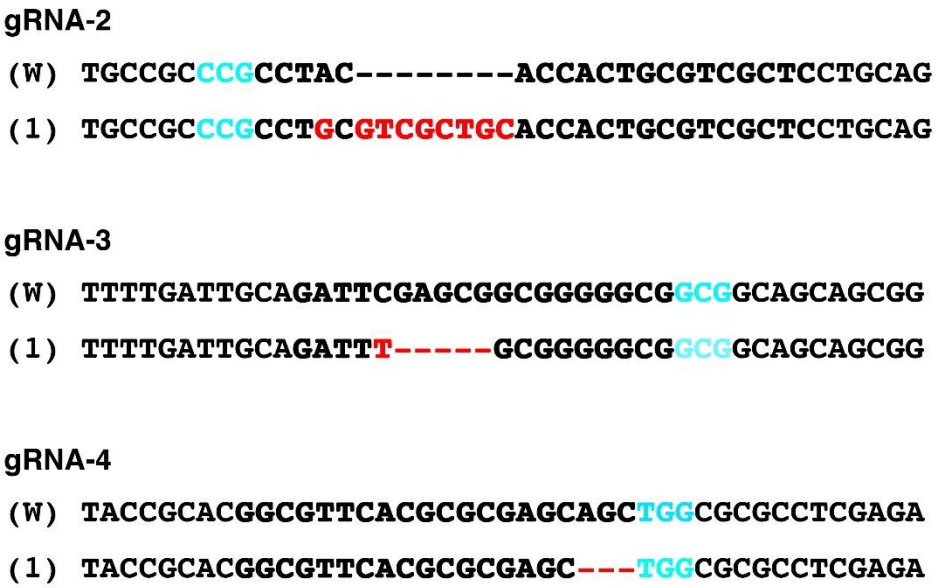

Figure 3. Sequences of the gRNA-2, gRNA-3, and gRNA-4 sites in WT and *Gb'eve* KO embryos. The sequences of WT and each KO embryo are presented by (W) and (1), respectively. The gRNA targeting sequence is presented as a bold black font. The PAM sequence is presented as a blue font. The sequence of indel mutation and base substitution is presented as a red font.

4.2. Strong phenotypes of *Gb'eve* KO mutants

Next, I observed in detail the phenotype of embryos in *Gb'eve* KO strains with indel mutations (Fig. 1C (1) and (2) and Fig. 3). At the hatching stage, *Gb'eve* KO embryos were significantly shorter by approximately 20% along the AP axis compared to WT embryos (Fig. 4A and B). *Gb'eve* KO embryos completely lacked gnathal, thoracic, and abdominal segments (Fig. 4A and B). The *Gb'eve* KO phenotype, which was called *eve*^{s} phenotype in this study, had a strong effect on segmentation. *Gb'eve*^{s} embryonic appendages, such as the antenna (and labrum, data not shown) in the forehead and the cercus in the telson (posterior terminal region), were normally formed; however, small prominences were formed in the ventral region (Fig. 4B). The shape of prominences in *Gb'eve*^{s} embryos did not correspond to those of any gnathal appendages (mandible, maxilla, and labium) and thoracic appendages (prothoracic, mesothoracic, and metathoracic legs) in WT embryos (Fig. 4C, D). One to three prominences were observed in the shortened trunk region of *Gb'eve*^{s} embryos. To examine segmental structure, I observed cuticular preparations of WT and *Gb'eve*^{s} embryos. In WT embryos, segmental boundaries were formed from the forehead to telson, and setae were formed on thoracic and abdominal segments between these boundaries (Fig. 4E). Two boundaries were identified on the posterior side of the forehead and anterior side of the telson in *Gb'eve*^{s} embryos. However, setae were not formed between them (Fig. 4F). Thus, *Gb'eve*^{s} embryos did not have the segmental structures of gnathal, thoracic, and abdominal segments, with *Gb'eve* clearly contributing to the segmentation of these segments and embryonic elongation.

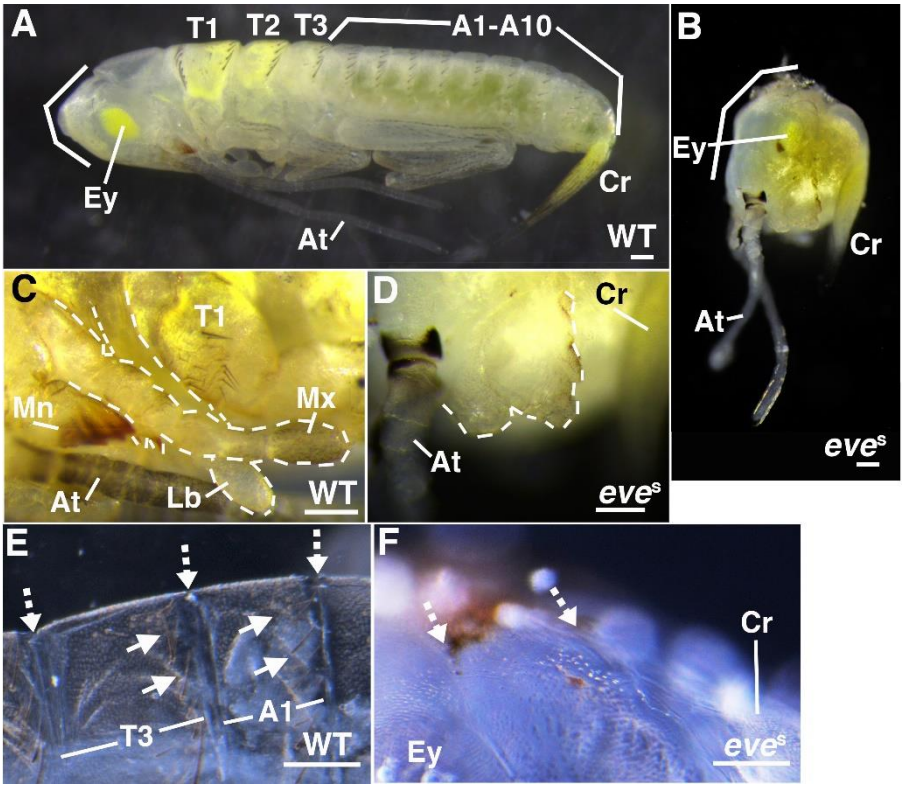

Figure 4. Structure of *Gb'eve* KO embryos with strong phenotypes. The anterior end is presented on the left side of all panels. Lateral view of WT (A, C) and *Gb'eve* KO (*eve*^{s}) (B, D) embryos at the hatching stage. (A, B) Frontal top part of embryos is shown by lines. (C) Head, gnathal, and T1 appendages of WT embryos. (D) Prominences between the antenna and cercus of *Gb'eve*^{s} embryos. Regions surrounded by dashed lines show maxilla, labium (C), and prominences (D) in WT and *Gb'eve*^{s} embryos, respectively. Cuticular preparations of WT (E) and *Gb'eve*^{s} (F) embryos showing the dorsal side of the lateral view. (E, F) White dotted arrows show segmental boundaries. White arrows show setae. (E) Cuticle of thoracic (T3) and abdominal (A1) segments of WT embryos. (F) There were two segmental boundaries on the posterior side of the forehead and the anterior side of the telson, but no setae in *Gb'eve*^{s} embryos. At, antenna; Ey, eye; Mn, mandible; Mx, maxilla; Lb, labium; T1-3, thoracic segment 1 to 3; A1-10, abdominal segment 1 to 10; Cr, cercus. Scale bar = 100 μm.

4.3. Moderate phenotypes of *Gb'eve* KO mutants

Unexpectedly, I detected several moderate phenotypes (which I called *eve*^{m} phenotype). The targeted sites, indel sizes, and the corresponding phenotypes were summarized in Table 3. Only in the *Gb'eve* KO strain with 5 bp deletion (Fig. 1C (3)), I observed the phenotypes in which thoracic and abdominal segments were clearly present in mutant embryos at the hatching stage. However, the number of segments and body size of the *Gb'eve*^{m} embryos were significantly reduced relative to WT embryos (Fig. 5A-C). The *Gb'eve*^{m} phenotype was thus hypomorphic compared to the *Gb'eve*^{s} phenotype. The total number of thoracic and abdominal segments of mutant embryos in the *Gb'eve*^{m} (3) strain was reduced to six (left side of the *Gb'eve*^{m} embryo; Fig. 5B), to four (left side of the *Gb'eve*^{m} embryo; Fig. 5C), or to three (right side of the *Gb'eve*^{m} embryo; Fig. 5C), while the total number of those segments in WT embryos is thirteen. *Gb'eve*^{m} embryos of the (3) strain were maximum 53% shorter along the AP axis compared to WT embryos (Fig. 5A and C); however, they were maximum 126% longer along the left-right axis (Fig. 5C). Therefore, the severity of reduction in the number of segments and body size in *Gb'eve*^{m} embryos was moderate compared to that in *Gb'eve*^{s} embryos.

Furthermore, I observed morphological structures of *Gb'eve*^{m} embryos in detail. In the *Gb'eve*^{m} embryo with the greatest numbers of segments, the total number of thoracic and abdominal segments differed on the left and right sides (Fig. 5B). This *Gb'eve*^{m} embryo had one large thoracic segment due to fusion of tergites, and had four or five abdominal segments (Fig. 5B). Moreover, the occiput (including gnathal segments) was shorter along the AP axis (Fig. 5B) compared to WT embryos (Fig. 5A). Its mandible and maxilla were normally formed, but the labium was missing (Fig. 5D and E). In addition, the prothoracic, mesothoracic and

metathoracic legs were reduced, and formed as two leg-like appendages in the shortened occiput and reduced thoracic region (Fig. 5F and G). On the other hand, the *Gb'eve*^{m} embryo with the least numbers of segments also had different total numbers of thoracic and abdominal segments on the left and right sides (Fig. 5C). This *Gb'eve*^{m} embryo had one thoracic segment and two to three abdominal segments (Fig. 5C). The occiput was not clearly identified in this *Gb'eve*^{m} embryos (Fig. 5C). All gnathal and thoracic appendages were lost except for a pair of appendage vestiges in the reduced thoracic region, probably due to severe fusion of the occiput and thoracic region (Fig. 5H). Because of these morphological structures, *Gb'eve*^{m} embryos exhibited hypomorphic phenotypes compared to the *Gb'eve*^{s} phenotype.

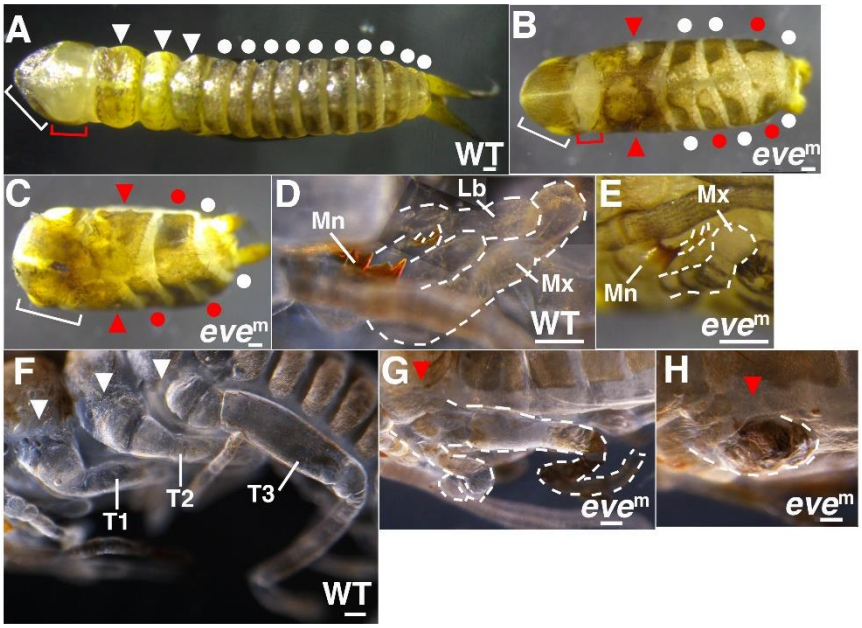

Figure 5. Structure of *Gb'eve* KO embryos with moderate phenotypes. The anterior end is presented on the left side of all panels. WT and *Gb'eve* KO (*eve*^{m}) embryos at the hatching stage in the dorsal (A-C), ventral (D, E), and lateral view (F-H). (A, D, F) WT embryos. (B, E, G) *Gb'eve*^{m} embryos with the greatest number of thoracic and abdominal segments in the *Gb'eve*^{m} (3) strain. (C, H) *Gb'eve*^{m} embryo with the least number of thoracic and abdominal segments in the *Gb'eve*^{m} (3) strain. (D, F-H) Cuticular preparations of WT and *Gb'eve*^{m} embryos. White arrowheads and dots show normal thoracic and abdominal segments, respectively. Red arrowheads and dots show abnormal thoracic and abdominal segments on the left and right side, respectively. Regions surrounded by dashed lines show maxilla (D, E), labium (D), two leg-like appendages (G), and single incomplete appendage (H) in WT and *Gb'eve*^{m} embryos, respectively. White and red brackets show forehead and occiput, respectively. Mn, mandible; Mx, maxilla; Lb, labium; T1–3, thoracic segment 1 to 3. Scale bar = 100 μm.

Table 3. Summary of *Gb'eve* KO strains established in this study.

Targeted site/exon	Molecular characterization	Phenotypic severity
gRNA-1/exon1	-1bp	Strong
gRNA-1/exon1	-7bp	Strong
gRNA-1/exon1	-5bp	Moderate
gRNA-1/exon1	+108bp	Moderate
gRNA-1/exon1	+473bp[a]	Moderate
gRNA-2/exon1	+8bp	Strong
gRNA-3/exon2	-5bp	Strong
gRNA-4/exon2	-3bp	Strong

[a]The indel size was not completely determined.

4.4. Establishment of *Gb'eve* knock-out strains by the CRISPR/Cas9 system and the ssODN donor template

These moderate phenotypes might imply that *Gb'eve* function remains slightly in *Gb'eve*^{m} embryos for some reason (e.g., mRNAs encoding at least part of functional domains might be transcribed through unexpected splicing; see discussion). To examine this hypothesis, I attempted to generate a *Gb'eve* KO strain by deleting the first to fifth exon of *Gb'eve* gene (about 23 kbp) with the CRISPR/Cas9 system using single-stranded oligonucleotide (ssODN) donor templates to stimulate homologous recombination (HR) (Gao et al., 2008; Huang et al., 2009) (Fig. 6). First, I newly designed a gRNA that determined specific sequence targeting the gRNA-5 site on the fifth exon, and an ssODN (Fig. 6), and injected gRNA-1, gRNA-5, and cas9 mRNA with different concentrations of ssODNs into eggs at 2-h AEL. Next, I performed genotyping of these G0 embryos. I randomly selected 10 G0 embryos from eggs injected with each concentration of ssODNs and extracted genomic DNA of them. I then performed genotyping PCR with designed primers (Fig. 6) and analyzed the rate of mutation frequency when injecting each concentration of ssODNs. For these G0 embryos, I could not detect the predicted genomic deletion of the *Gb'eve* gene between two gRNA target sites by ssODN-mediated HR (Fig. 6); however, I could detect the genomic deletion between both sites by nonhomologous end joining (NHEJ). The rate of frequency of the genomic deletion by NHEJ was 10, 30, 40, and 50% when injecting 0, 24, 240, and 2000 ng/μl ssODNs, respectively. Thus, ssODNs might assist the genomic deletion of about 23 kbp by NHEJ. Accordingly, I predicted the genomic deletion by NHEJ would be transmitted to G1 crickets.

I also evaluated whether these mutations would be transmitted to G1 crickets,

based on the rate of the mutation frequency. The survival rates of fertile G0 adults were 8, 15, and 11% when injecting 24, 240, and 2000 ng/μl ssODNs, respectively (Table 4). I then performed genotyping to specify G0 founders yielding offsprings with the targeted deletion and estimated germline transmission rates when injecting each concentration of ssODNs. First, fertile G0 adults were crossed with WT adults. Then, genomic DNA was extracted from 25 G1 embryos of each crossed adult pair. I then performed genotyping PCR with the designed primers (Fig. 6) to detect the targeted event. I could not detect the genomic deletion between two gRNA target sites by ssODN-mediated HR and NHEJ in these G1 embryos. That is, the germline transmission rates were 0% in G0 founders yielding offsprings with the targeted event when injecting any concentration of ssODNs (Table 4). Thus, it might be difficult to transmit genomic deletions of about 23 kbp to the progeny in crickets. However, PCR analysis using primer1-F and 1-R (Fig. 1A) was able to detect mutant alleles with insertion mutations at the gRNA-1 site in the G1 embryos when injecting 240 and 2000 ng/μl ssODNs, respectively (Fig. 7). I then performed sequence analysis of these PCR products and confirmed insertion mutations of 108 bp or approximately 490 bp, which were probably irregular integration of the ssODN sequence via erroneous repair at the gRNA-1 site (Fig. 8). Therefore, germline transmission rates were 0, 4, and 13% in G0 founders yielding offsprings with the insertion mutations when injecting 24, 240, and 2000 ng/μl ssODNs, respectively (Table 4).

After the G1 embryos of each G0 mutant line hatched, I performed genomic screening of G1 heterozygous mutants by genotyping PCR with the specific primers (Fig. 1A). I detected mutant alleles with the insertion mutations at the gRNA-1 site in G1 heterozygous nymphs (Fig. 7). Potential *Gb'eve* hemizygous mutant embryos, which exhibit apparent morphological phenotype (see Fig. 9), were obtained through interbreeding *Gb'eve*

heterozygous females and WT males. In the potential mutant embryos, I then performed sequence analysis of induced mutations and confirmed the same insertion mutations as the sequence of G1 embryos (Fig. 8). Consequentially, I was not able to obtain the *Gb'eve* KO strains with expected genomic deletion mutation; however, I did isolate two *Gb'eve* KO strains with the irregular integration of the ssODN sequence via erroneous repair at the gRNA-1 site (Fig. 8 and Table 3 and 4).

The mutant embryos in these two strains (strains (4) and (5) in Fig. 8) had *Gb'eve*^{m} phenotypes (Fig. 9). The *Gb'eve*^{m} embryos in (4) and (5) strains were more weakly or strongly affected, respectively, regarding the segmentation of gnathal to abdominal segments and embryonic elongation compared to mutant embryos in the (3) strain (Fig. 5B, C, E, G, H, and 9). In particular, the total numbers of thoracic and abdominal segments in the mutant embryos of *Gb'eve*^{m} (4) and (5) strains were reduced to 11–7 and 6–2, respectively, while that of the *Gb'eve*^{m} (3) strain was reduced to 6–3 (Fig. 9F). The total number of these segments in the most frequently observed *Gb'eve*^{m} embryos was 6 for the *Gb'eve*^{m} (3) strain at 78%, 9 for the (4) strain at 40%, and 3 or 4 in the (5) strain at 40% each (Fig. 9F). Thus, the number of lost segments in the gnathal to abdominal region varies among KO individuals in a *Gb'eve*^{m} strain and among the *Gb'eve*^{m} strains. Of note, the posterior gnathal to first abdominal (A1) segments were more sensitively affected in *Gb'eve* KO embryos compared to the remaining segments (Fig. 9A).

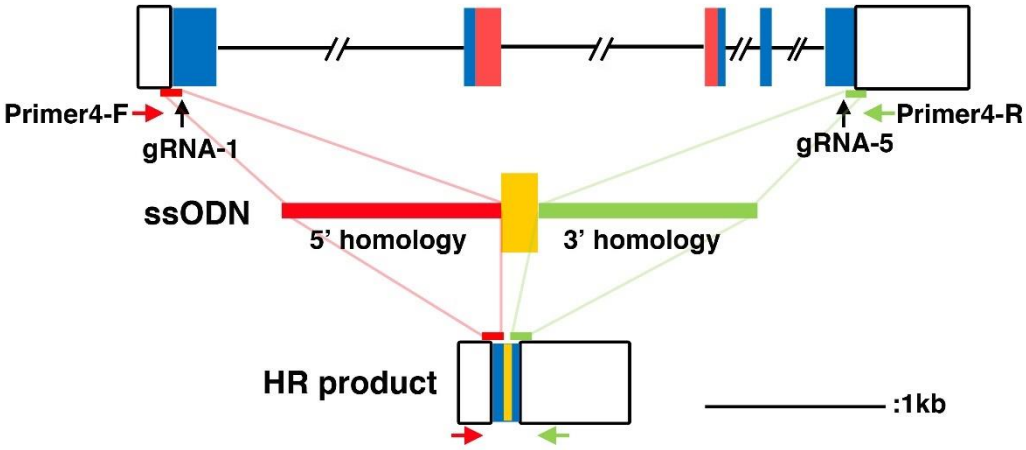

Figure 6. Schema of the genomic deletion of *Gb'eve* induced by CRISPR/Cas9 and ssODN. Top row: five boxes indicate the five exons; black lines indicate the four introns. The homeodomain coding region is presented in a red box. The translated and untranslated regions are presented in blue and white boxes, respectively. The gRNA target sites are located on the sense strand of exon1 (gRNA-1) and anti-sense strand of exon5 (gRNA-5). Primer4-F and primer4-R were used to anneal to the upstream and downstream regions of the gRNA-1 and gRNA-5 sites, respectively. Middle row: ssODN donor template including 60 nt homologous arms (red and green lines) flanking the 13 nt insertion sequence (yellow box). These homologous arms correspond to sequences immediately adjacent to the DSB sites (black arrows). For additional details, see supplemental methods. Bottom row: homologous recombination (HR) product indicates the predicted genomic deletion of *Gb'eve* between the DSB sites by ssODN-mediated HR.

Table 4. Germline transmission rates in G0 crickets injected with ssODNs

Concentration of gRNAs and Cas9 mRNA (ng/μl)	Concentration of ssODN (ng/μl)	Injected embryos	% (no.) fertile adults	% (no.) founders yielding deletion event[a]	% (no.) founders yielding insertion mutation[b]
50/100	24	69	8(5/59)	0(0/5)	0(0/5)
50/100	240	202	15(28/192)	0(0/28)	4(1/28)[c]
50/100	2000	84	11(8/74)	0(0/8)	13(1/8)[d]

[a]The rate of founders yielding the targeted event represents percentage of injected crickets producing progeny in which the genomic deletion occurred (founders) per fertile adults.

[b]The rate of founders yielding the insertion mutation represents percentage of injected crickets producing progeny in which the insertion mutations occurred at the gRNA-1 site (founders) per fertile adults.

[c]Insertion mutation of 108 bp occurred at the gRNA-1 site.

[d]Insertion mutation of approximately 490 bp occurred at the gRNA-1 site.

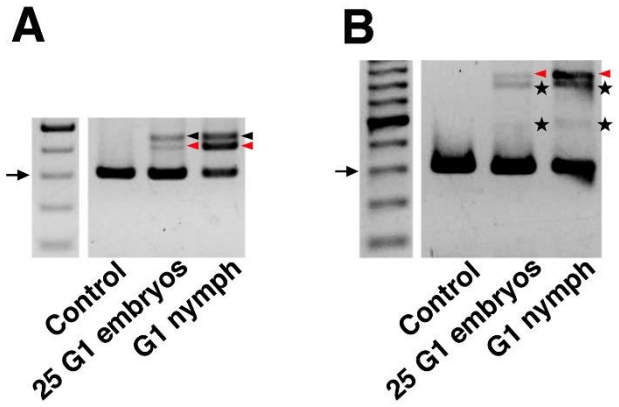

Figure 7. Genomic screening of G1 embryos and nymphs with mutant alleles by genotyping PCR targeting the gRNA-1 site. (A) G1 embryos and nymphs from fertile G0 adults injected with 240 ng/μl ssODNs. (B) G1 embryos and nymphs from fertile G0 adults injected with 2000 ng/μl ssODNs. Red and black arrowheads indicate the presence of homoduplex PCR products from mutant alleles and heteroduplex PCR products from WT and mutant alleles, respectively. The asterisk indicates nonspecific PCR products were amplified from mutant alleles because of multiple repetitive sequences. Arrow indicates 300 bp sized marker.

Figure 8. Sequences of the gRNA-1 site in *Gb'eve* KO embryos with the irregular integration of the ssODN. The sequence in WT is presented by (W). The sequences in each KO embryo at injecting 240 and 2000 ng/μl ssODNs are presented by (4) and (5), representing insertion mutations of 108 bp or approximately 490 bp, respectively. The gRNA targeting sequence is presented in a bold black font. The PAM sequence is presented in a blue font. The sequence of insertion mutation and base substitution is presented in a red font. I could not determine all of the nucleotide sequece throuhgout the insertion (ca. 490 bp) in the (5) strain, because the sequence of insertion mutation (5) was GC rich and included multiple repetitive sequences. The undetermined region (~20 bp?) was indicated by N (yellow).

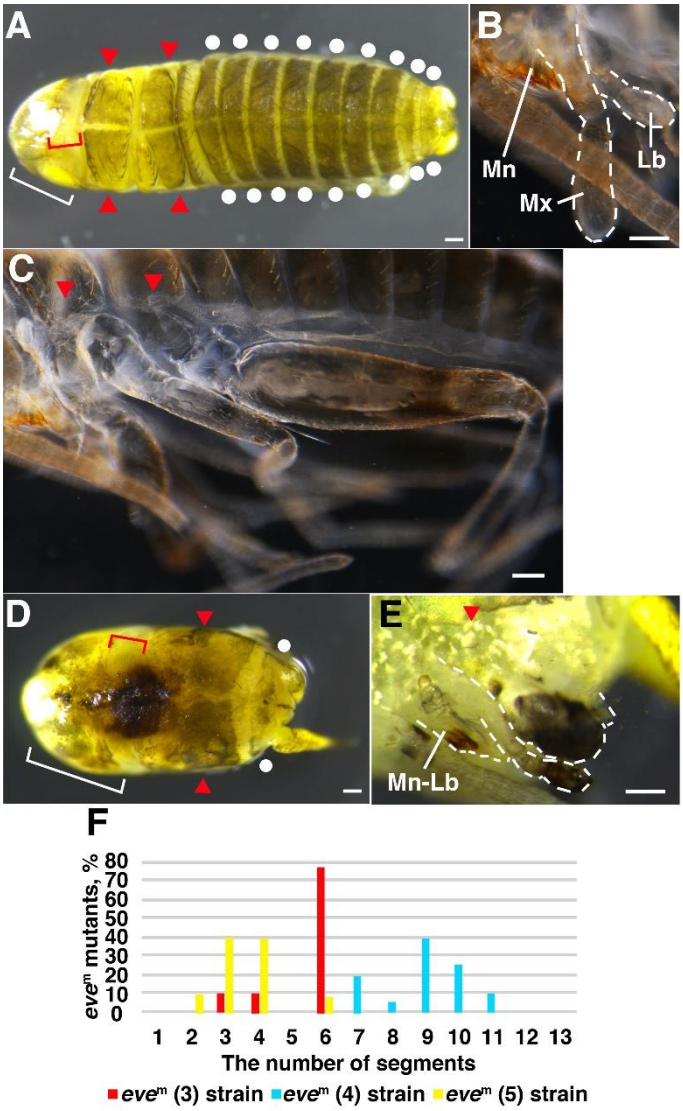
A
B
Mn
Lb
Mx
C
D
E
Mn-Lb
F
eve^m mutants, %
80
70
60
50
40
30
20
10
0
1 2 3 4 5 6 7 8 9 10 11 12 13
The number of segments
eve^m (3) strain
eve^m (4) strain
eve^m (5) strain

Figure 9. Phenotypes of *Gb'eve*^{m} embryos with the irregular integrations of the ssODN. The anterior end is presented in the left panels. *Gb'eve*^{m} embryos with insertion mutations (see Fig. 8 (4) (5)) at the hatching stage in the dorsal view (A, D) and lateral view (B, C, D). (A–C) *Gb'eve*^{m} embryos with the greatest thoracic and abdominal segments in *Gb'eve*^{m} (4) strain. These *Gb'eve*^{m} embryos had two thoracic segments and nine abdominal segments. (B, C) In the appendicular cuticles of the *Gb'eve*^{m} embryos, gnathal appendages (mandible, maxilla, and labium) and thoracic appendages (T1 and T3 legs) were formed normally, but the T2 leg was slightly dwarfed on shortened occiput and reduced thoracic region, as compared with other legs. (D, E) *Gb'eve*^{m} embryos with the least thoracic and abdominal segments in *Gb'eve*^{m} (5) strain. These *Gb'eve*^{m} embryos had one thoracic segment and one abdominal segment. (D) The *Gb'eve*^{m} embryos in the (5) strain were maximum 49% shorter along the AP axis; however, they were maximum 133% longer along the left-right axis, as compared with WT embryos (Fig. 5A). (E) In the appendages of the *Gb'eve*^{m} embryos, the mandible, maxilla, and labium were reduced and formed as single joined gnathal appendage on a shortened occiput region. Then, all legs were reduced and formed as single incomplete appendage on the reduced thoracic region. (A, D) The length of the occiput along the AP axis in these *Gb'eve*^{m} embryos was shorter than that in WT embryos (Fig. 5A). Red arrowheads show abnormal thoracic segments. White dots show normal abdominal segments. The region surrounded by white dashed line shows gnathal or thoracic appendages. White and red brackets show forehead and occiput, respectively. Mn, mandible; Mx, maxilla; Lb, labium; T1–3, thoracic segment 1 to 3. Scale bar = 100 μm. (F) Rate of *Gb'eve*^{m} embryos with variable total numbers of thoracic and abdominal segments in each strain. The number of those segments in WT embryos is 13. The number of segments reduced to 6–3 in the *Gb'eve*^{m} (3) strain (n = 9), 11–7 in the *Gb'eve*^{m} (4) strain (n = 20), and 6–2 in the *Gb'eve*^{m} (5) strain (n = 25), respectively.

4.5. Expression of appendage and segment maker genes in *Gb'eve* KO mutants

I investigated how the expressions of appendage marker gene *Gryllus Distal-less* (*Gb'Dll*) and segment marker gene *wingless* (*Gb'wg*) were affected in *Gb'eve*^{s} embryos. *Gb'Dll* expressions were detected in the antenna, labrum, maxilla, labium, legs, and cerci of WT embryos at embryonic stage (ES) 9, but were not detected in the mandible (Fig. 10A). *Gb'Dll* expression was observed in all of the prominences of *Gb'eve*^{s} embryos at ES 9, in addition to the antenna, labrum, and cerci (Fig. 10B). The expression pattern in the anterior prominences of *Gb'eve*^{s} embryos was similar to that in the maxilla and labium of WT embryos, whereas the pattern of expression in the posterior prominences of *Gb'eve*^{s} embryos was similar to that of the trunk-proximal portion of legs in WT embryos (Fig. 10A-D). Thus, the prominences in *Gb'eve*^{s} embryos are likely to be vestiges of gnathal and thoracic appendages.

In WT embryos at ES 9, *Gb'wg* was expressed in the segmental boundaries of the trunk segments (Fig. 10E). *Gb'wg* expression was also detected in the foregut and hindgut (Fig. 10E). In contrast, in *Gb'eve*^{s} embryos at ES 9, *Gb'wg* expression was not detected in the trunk region, but remained in the foregut and hindgut (Fig. 10F). Thus, *Gb'eve*^{s} embryos likely failed to form segmental boundaries from the mandibular segment to the tenth abdominal segment. The remaining expression in the foregut and hindgut supports that the anterior and posterior terminal regions were properly differentiated in *Gb'eve*^{s} embryos (Fig. 10F).

I also examined the effect on *Gb'eve*^{m} on *Gb'wg* expression. *Gb'wg* expression was clearly present in the thoracic and abdominal segments and gnathal and thoracic appendages of mutant embryos at ES 9, particularly in the *Gb'eve*^{m} (3) and (4) strains (Fig.

10G). However, the number of segments and appendages declined asymmetrically, probably due to their fusion or deletion (Fig. 10G). *Gb'wg* expression in mutant embryos at ES 9, particularly in the *Gb'eve*^{m} (3) and (5) strains, was not detected between the reduced gnathal region, including normal mandible and maxilla, and reduced abdominal region (Fig. 10H). Thus, the pattern of *Gb'wg* expression in *Gb'eve*^{m} embryos resembled that of *Gb'eve*^{s} embryos, as the phenotype of the *Gb'eve*^{m} embryos became more severe (Fig. 10F). In the most severe case, the *Gb'eve*^{m} embryo clearly failed to form segmental boundaries from the labium to eighth abdominal segment.

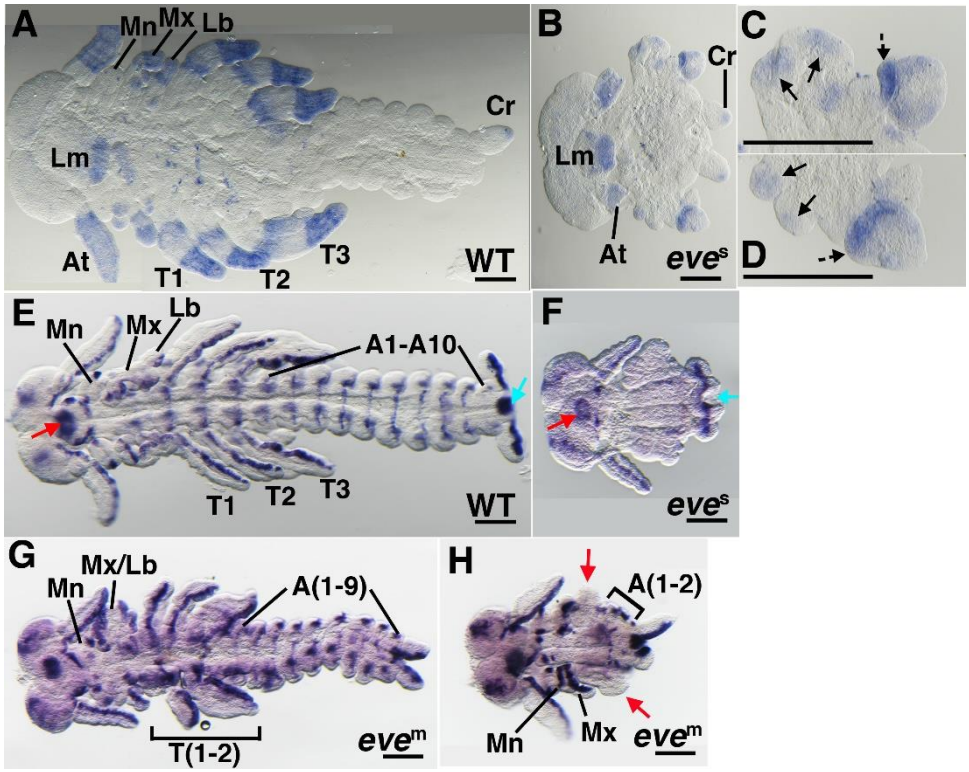

Figure 10. Expression of appendage and segment marker genes in *Gb'eve* KO embryos. The anterior end is presented on the left side of all panels. Expression patterns of *Gb'Dll* in WT (A) and *Gb'eve*^{s} (B-D) embryos at ES 9 in the ventral view. Note that one of two cerci (A) or parts of both antennae (B) are cleaved from the embryos. (C, D) Black arrows and dotted arrows show *Gb'Dll* expression at the anterior and posterior prominences, respectively. Expression patterns of *Gb'wg* in WT (E), *Gb'eve*^{s} (F), and *Gb'eve*^{m} (G, H) embryos at ES 9 in the ventral view. (E, F) Red and blue arrows show the foregut and hindgut, respectively. (G) *Gb'eve*^{m} embryos in the (3) and (4) strains. (H) *Gb'eve*^{m} embryos in the (3) and (5) strains. Red arrows indicate segments and appendages where *Gb'wg* expression was not detected. At, antenna; Lm, labrum; Mn, mandible; Mx, maxilla; Lb, labium; T1-3, thoracic segment 1 to 3; A1-10, abdominal segment 1 to 10; Cr, cercus. Scale bar = 100 μm.

4.6. Expression of Hox genes in *Gb'eve* KO mutants

I examined the effects of *Gb'eve* KO on Hox gene expression. Expression of the *Gryllus Sex combs reduced* (*Gb'Scr*) ortholog was detected in the labium (Lb) and prothoracic (T1) segments of WT embryos at ES 9 (Fig. 11A). In *Gb'eve*^{m} embryos at ES 9, *Gb'Scr* expression was similar to that of WT embryos; however, the sites of expression became restricted due to the fusion of Lb and T1 segments (Fig. 11B). In *Gb'eve*^{s} embryos at ES 9, *Gb'Scr* was expressed in the middle region of embryos (Fig. 11C). *Gryllus abdominal A* (*Gb'abd-A*) ortholog expression was detected between the first and ninth abdominal segments of WT embryos at ES 9 (Fig. 11D). In *Gb'eve*^{m} embryos, *Gb'abd-A* was expressed in the remaining abdominal segments (Fig. 11E). In *Gb'eve*^{s} embryos, *Gb'abd-A* was expressed in the more posterior region of embryos (Fig. 11F). Interestingly, these Hox genes were expressed in *Gb'eve*^{s} embryos, despite their lacking gnathal to abdominal segments.

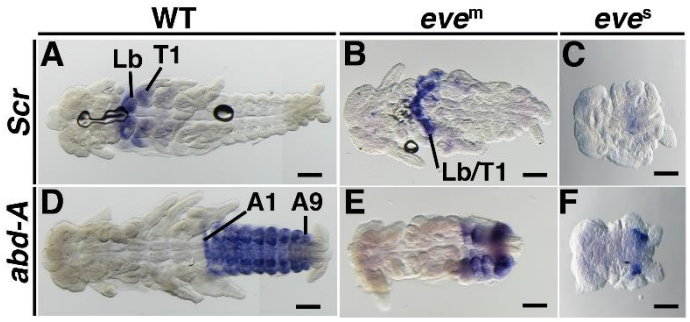

Figure 11. Expression of Hox genes in *Gb'eve* KO embryos. The anterior end is presented on the left side of all panels. The embryos in all panels are shown in ventral view. Expression patterns of *Gb'Scr and Gb'abd-A* in WT (A, D), *Gb'eve*^{m} (B, E) and *Gb'eve*^{s} (C, F) embryos at ES 9. (A, D) In WT embryos, *Gb'Scr* was expressed in Lb and T1 segments, and *Gb'abd-A* was expressed from A1 to A9 segments. (B, E) In *Gb'eve*^{m} embryos, *Gb'Scr* was expressed in one segment of the fused Lb/T1 segments, and *Gb'abd-A* was expressed in the reduced abdominal segments. (C, F) In *Gb'eve*^{s} embryos, *Gb'Scr* was expressed in the middle region of the embryo, and *Gb'abd-A* was expressed in a more posterior region of the embryo than the expression region of *Gb'Scr*. Note that parts of both antennae are cleaved from the embryos. Lb, labium; T1, thoracic segment 1; A1–9, abdominal segment 1 to 9. Scale bar = 100 μm.

5. Discussion

This study aimed to advance phenotypic analyses and to examine *Gb'eve* function using *eve* knock-out cricket strains. My results showed that *Gb'eve*^{s} embryos with indel mutations at each gRNA targeted site (Fig. 1C and 3) had an amorphic (genetic null) mutant phenotype, which was more severe than *eve* RNAi phenotypes (Mito et al., 2007). In contrast, *Gb'eve*^{m} embryos with indel mutations only at the gRNA-1 site (Fig. 1C and 8) had a hypomorphic mutant phenotype. Thus, both phenotypes represent a series of phenotypes because the segments of *Gb'eve* KO embryos were successively affected like *Drosophila eve* mutants (Macdonald et al., 1986). At present, I do not know how the hypomorphic phenotypes were generated in the obtained KO strains in spite of the fact that induced mutations did indeed cause frameshifts in the *eve* gene in the KO strains. One potential explanation is that mRNAs encoding at least part of functional domain, such as the homeodomain and Groucho interacting domain, might be transcribed through alternative splicing escaping the induced mutation, and in consequence, incomplete but functional Eve proteins might be translated in *Gb'eve*^{m} embryos. In *Drosophila*, it is reported that *eve* mutants lacking the Groucho interacting domain show the specific hypomorphic phenotype (Fujioka et al., 2002; Kobayashi et al., 2001). Furthermore, the fact that the hypomorphic phenotypes of *Gb'eve* RNAi embryos (Mito et al., 2007), in which *eve* expression could not in principle be completely suppressed, are greatly similar to *Gb'eve*^{m} phenotypes supports my hypothesis.

5.1. *Gb'eve* does not have a gap-like function

I observed that the *Gb'eve* amorphic embryo was significantly shorter along the AP axis (Fig. 4B), and did not have body segments (Fig. 4F) or segmental expression of the

marker gene (*Gb'wg*) in the shortened trunk region (Fig. 10F). At first glance, this phenotype appears to reflect *Gb'eve* action as a gap gene, implying the loss of multiple contiguous body segments. However, this seems unlikely, rather, *Gb'eve* KO phenotypes might result from defects in embryonic elongation and formation of the segmental boundaries in the gnathal to abdominal region. This suggestion is supported by the fact that potential vestiges of gnathal and thoracic appendages with expression of the appendage marker gene (*Gb'Dll*) were formed in the trunk region of the amorphic embryos (Fig. 10B-D). Second, the Hox genes, *Gb'Scr* and *Gb'abd-A*, were expressed in the trunk region of the amorphic embryos, and maintained a positional order of expression sites between these genes (Fig. 11). Since the expression domain of each Hox gene was severely reduced, the proper regulation of these genes could be defective in the *Gb'eve* KO embryos. However, the stepwise reduction of the expression domain from the wild type to moderate and, subsequently, strong phenotypes indicates that the regulation of expression is basically maintained. Thus, the shortened trunk region in the amorphic embryos was caused by embryonic elongation defects, rather than the loss of contiguous body segments. Overall, *Gb'eve* may not act in a gap-gene like manner, but may contribute to embryonic elongation and the formation of segmental boundaries in the gnathal to abdominal region. In addition, since the posterior terminal region (including cercus) was clearly formed in *Gb'eve* null mutants, *Gb'eve* may not be involved in formation of the posterior terminal region.

5.2. Nonuniform requirements of *Gb'eve* activity among segments

In the present study, phenotypic continuity was observed between *eve* hypomorphs and amorphs in *Gryllus*, as the number of missing body segments increased continuously, reaching a maximum in amorphs (Fig. 4, 5, and 9). In addition, the posterior gnathal to A1

segments were more sensitive to *Gb'eve* KO compared to other segments (Fig. 9). These segments might represent the highest requirement for *Gb'eve* activity in the formation of the segmental boundaries. Thus, the requirements of *Gb'eve* activity could be nonuniform between anterior and posterior segments during segmentation.

5.3. Evolution of *eve* function

The *Gb'eve* null phenotype detected in the present study was reminiscent of the lawn phenotype of *Drosophila eve* amorphic embryos, which also has a defect in embryonic elongation and the formation of the segmental boundaries in the gnathal to abdominal region (Coulter and Wieschaus, 1988; Macdonald et al., 1986). Thus, this essential function of the *eve* gene (designated as "whole segment regulation") might be conserved between *Gryllus* and *Drosophila* and thus could be ancestral to insects (Fig. 12). Recent studies suggested that the pair-rule gene network in segmentation might have shifted from short germ insects to long germ insects, without an essential change (Clark, 2017; reviewed in Clark et al., 2019). My finding seems to be consistent with such a view.

The nonuniform requirement, which is assumed from the phenotypic continuity of *Gb'eve*, also reminds *Drosophila eve* mutants. In *Drosophila*, it is suggested that Eve might act at different concentration thresholds in each segment (Fujioka et al., 1995; Lawrence and Johnston, 1989). *Gryllus* Eve might also be involved in the concentration-dependent activity in segmentation, as well as *Drosophila* Eve. However, recent reports reveal that *Drosophila* Eve regulates different downstream genes through shifts in its expression domains, proposing that the action of Eve could be explained without assuming the concentration-dependent activity (Clark, 2017; reviewed in Clark et al., 2019). At present, it is unclear which mechanism *Gb'eve* hypomorphic phenotypes reflect. It is necessary to clarify regulatory

relationships between *Gb'eve* and its downstream genes.

I also compared the function of *Gryllus eve* with other insects for which functional analyses of *eve* orthologs have been performed. My hypothesis that involvement in whole segment regulation might be an ancestral *eve* function for insects appears to be supported by comparisons with other insects (Fig. 12). In *Tribolium* and *Bombyx*, this function may be conserved because knockdown of *eve* in these insects causes the asegmental phenotypes corresponding to the *Gb'eve* null mutant phenotype (Choe et al., 2006; Nakao, 2015). In *Nasonia*, morpholino-induced knockdown of *eve* causes posterior truncation of the embryo and loss or fusion of the anterior segments in the embryo (Rosenberg et al., 2014). The phenotype reported in the previous study appears to be due only to relatively weak knockdown effects, but given the shortening of the embryo and loss of all segmental boundaries in the phenotype, it is consistent with the conservation of whole segment regulation as *eve* funtion. *Oncopeltus eve* knockdown, on the other hand, causes a complete deletion of the gnathal through abdominal region, which is much more severe than the null phenotype in *Gryllus* and *Drosophila* (Liu and Kaufman, 2005; Macdonald et al., 1986). The *Oncopeltus eve* may function as a gap gene throughout the embryo, beyond its involvement in embryonic elongation as suggested in *Gryllus* (Liu and Kaufman, 2005). The *eve* function of whole segment regulation might have been modified in the *Oncopeltus* lineage.

Considering the above, the whole segment regulation is likely to be an ancestral funtion for *eve* in insects, and thus the regulatory network involving *eve* for this function might have been acquired at least at the stage of the common ancestor of *Gryllus* and *Drosophila* (Fig. 12). In the course of insect evolution, some lineages might have added new functions to *eve* genes, such as gap gene-like function in *Oncopeltus* (Fig. 12). Elucidation and comparative analyses of regulatory networks involving *eve* in *Gryllus* and other insects would

provide a deeper understanding of the evolution of *eve* function in segmentation.

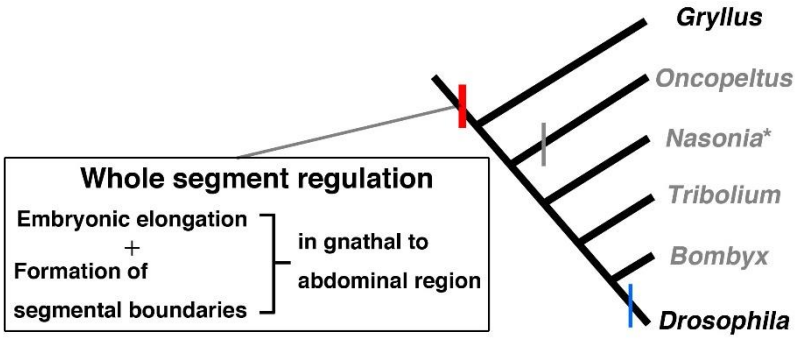

Figure 12. Evolution of *eve* functions in various insects. This phylogenetic tree is based on Misof et al., (2014) and Schwentner et al., (2017). Red line indicates the acquisition of the whole segment regulation (function on the embryonic elongation and the formation of the segmental boundaries in the gnathal to abdominal region) by *eve*. Gray line indicates that *Oncopeltus eve* might have been involved in gap gene-like function in addition to the whole segment regulation. Blue line indicates the acquisition of refined pair-rule function in the lineage leading to *Drosophila*. Asterisk: the gnathal segments in *Nasonia* is structurely unclear and *eve* function on those segments is ambiguous (Rosenberg et al., 2014). Black and gray fonts indicate insects whose *eve* function has been analyzed by genetic mutations and RNAi or Morpholino, respectively.

6. Future studies

In this thesis, I performed the genome modification using the CRISPR/Cas9 system and ssODN by injecting the Cas9 ribonucleoprotein (RNP) complex into cricket eggs. However, for the functional analysis, it takes a lot of time and effort to establish knock-out strains for a target gene. To resolve this issue, a potential technology termed Receptor-Mediated Ovary Transduction of Cargo (ReMOT Control) was first developed using mosquitoes as a model, delivering the Cas9 RNP to oocytes by intrathoracic injection of the body cavity of adult females (Chaverra-Rodriguez et al., 2018). The ReMOT Control is easier for injecting Cas9 RNP than egg injection, and also has an advantage in shortening experiment time because we can obtain knock-out phenotypes in the progenies of injected adult females via mutagenesis in the ovary. Thus, using this technology, the time and effort required for the functional analysis would be greatly reduced.

This technology was succeeded in holometabolous and hemimetabolous insects (Chaverra-Rodriguez et al., 2020; Heu et al., 2020; Shirai and Daimon, 2020). In these studies, in order to deliver the Cas9 RNP to oocytes, short peptide fragment of *Drosophila melanogaster* Yolk protein 1 or *Bemisia tabaci* Vitellogenin was used as a ligand binding to vitellogenin receptors on the oocyte membrane and was fused to N-terminus of the Cas9 protein. At present, N-terminal sequences of two *Gryllus vitellogenin* gene, which I called *Gb'vtg*231 and *Gb'vtg*296, were cloned based on 700 aa vitellogenin N region from *Schistocerca gregaria* vitellogenin B (QGR25458.1). I identified the homologous sequences from vitellogenin genes of other insects (*B. tabaci*（XP_018897090.1 and XP_018897089.1）, *N. vitripennis* (XP_001607388.1), *T. castaneum* (EFA11425.1), *A. gambiae* (AAF82131.1)) using the amino acid sequences of two cloned cDNA. The target peptide used in the ReMOT

Control in *B. tabaci* (Heu et al., 2020) was included within the sequence homologous to *Gb'*Vtg231 and *Gb'*Vtg296 (Fig. 13). Particularly, a methionine and glutamic acid were completely conserved in the target peptide, and amino acids downstream of the target peptide also highly conserved among Vtg sequences of the most insects (Fig. 13). Thus, I designed 71 aa *Gb'*Vtg231 which was highly homologous to *B. tabaci* Vitellogenin and included the target peptide in *B. tabaci*, as a new target peptide suitable for *G. bimaculatus* (Fig. 13). To achieve the ReMOT Control in *Gryllus*, I have planned to inject the RNPs complexed with target gRNA and Cas9 protein fusing the target peptide fragment of *Gb'*Vtg231 into female crickets under various conditions (e.g., timing of the Cas9 RNP injection during nymph to adult stages), and to optimize the condition based on the rate of mutation frequency in the progenies. This technology would allow us to perform large-scale analysis of downstream genes of *Gb'eve* rapidly, leading to further understanding of the evolution in segmentation mechanisms.

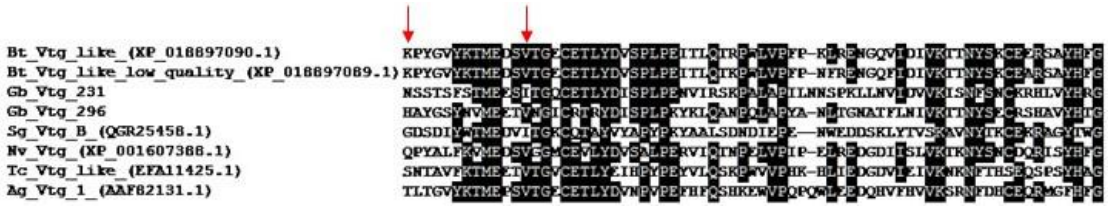

Figure 13. Specification of the target peptide in *Gb'*Vtg. *S. gregaria* vitellogenin B (QGR25458.1), *B. tabaci* predicted vitellogenin like (XP_018897090.1), *B. tabaci* predicted vitellogenin like (XP_018897089.1), *N. vitripennis* vitellogenin (XP_001607388.1), *T. castaneum* vitellogenin like (EFA11425.1), *A. gambiae* vitellogenin 1 (AAF82131.1) were aligned with *Gb'*Vtg231 and *Gb'*Vtg296 using ClustalW (https://www.genome.jp/) and adjusted by eye. The sequence located between red arrows (KPYGVYKTMEDSV) is the target peptide used in the ReMOT Control in *B. tabaci* (Heu et al., 2020). Conserved amino acid residues are shown with black-shaded frames.

7. Experimental procedures

Animals

Nymphs and adults of the *Gryllus bimaculatus* white-eyed mutant strain (Mito and Noji, 2008; Ylla et al., 2021) were reared at 30 °C and 50% relative humidity. Fertilized eggs of this strain were collected with wet kitchen towels and incubated at 30 °C in a plastic dish. *Gryllus* embryogenesis was based on the stages described by Donoughe and Extavour (2015).

Identification of the gene structure of *Gryllus eve* ortholog and measurement of gene copy number

The putative *eve* gene structure was identified in the sequencing, assembly, and annotation data of the *G. bimaculatus* genome (Ylla et al., 2021; DDBJ Accession Number, PRJDB10609) by performing a BLAST search using the previously isolated *eve* cDNA sequence (Mito et al., 2007; DDBJ Accession Number, AB120736). To measure the gene copy number, quantitative polymerase chain reaction (PCR) was performed using a power SYBR Green PCR Master Kit (Applied Biosystems) and an ABI 7900 Real-Time PCR System (Applied Biosystems), as described previously (Nakamura et al., 2008). We used *Gryllus β-actin* gene as the internal standard. The used primers in this experiment are listed in Table 5.

Table 5. Primers used in this study.

Primer name	Primer sequence (5'-3')	Primer purpose
gRNA-1 gF	ATAGCATATCCCGGCGTCCGTGC	Preparation of gRNA template
gRNA-1 gR	AAACGCACGGACGCCGGGATATG	Preparation of gRNA template
gRNA-2 gF	ATAGAGCGACGCAGTGGTGTAGG	Preparation of gRNA template
gRNA-2 gR	AAACCCTACACCACTGCGTCGCT	Preparation of gRNA template
gRNA-3 gF	ATAGATTGCAGATTCGAGCGGCG	Preparation of gRNA template
gRNA-3 gR	AAACCGCCGCTCGAATCTGCAAT	Preparation of gRNA template
gRNA-4 gF	ATAGGCATTCACGCGCGAGCAGC	Preparation of gRNA template
gRNA-4 gR	AAACGCTGCTCGCGCGTGAATGC	Preparation of gRNA template
gRNA-5 gF	ATAGGGCTGGAAGAGCTTGGGCG	Preparation of gRNA template
gRNA-5 gR	AAACCGCCCAAGCTCTTCCAGCC	Preparation of gRNA template
Primer1-F	CGCCGTTTGCTCAGGTTCTAGAGAG	Genotyping PCR for screening
Primer1-R	CGTTTTTCTCGCGACCGTTAGACCT	Genotyping PCR for screening
Primer2-F	CCAATCGGTAAAGCTTCCAG	Genotyping PCR for screening
Primer2-R	CGCGACACGTAGTTCTCCTT	Genotyping PCR for screening
Primer3-F	AACGATTGTGATTTTGATTGCAGAT	Genotyping PCR for screening
Primer3-R	AAATACCTTGATGGTGGACTCTGG	Genotyping PCR for screening
Primer4-F	TCCCTCCCCCACTGTTTAGT	Genotyping PCR for screening
Primer4-R	CTCTGTGGCAGGTTTGTGAA	Genotyping PCR for screening
eve-F	AATAAGAACGTGCACAAGACGAC	qPCR
eve-R	GAAAAATGTGCGCTCACTCTC	qPCR
act-F	TTGACAATGGATCCGGAATGT	qPCR
act-R	AAAACTGCCCTGGGTGCAT	qPCR
ssODN	ATCTGAAAATGCAGCAGTTCAGGTTGTTGGAGTCT CCGCCGCAGCATATCCCGGCGTCCGAATAAATAG ATAGCCAAGCTCTTCCAGCCCTACAAGTCCGACAT CTCGGAGCGAGCGTAAGTTCGCGACCGCT	Donor template for genomic deletion

Preparation of Cas9 mRNA, gRNA, and ssODN

Cas9 mRNA was synthesized using a mMESSAGE mMACHINE T7 Ultra Kit (Ambion) according to the manufacturer's instruction and previously described methods (Horch et al., 2017). Using Poly (A) Tailing Kit (Ambion), poly A was added to its 3' termini. After purification, a 2 μg/μl volume was prepared with an injection solution, and was preserved at -80 °C. Using the website "focas" (http://focas.ayanel.com/), gRNAs were designed (Osakabe et al., 2016). Out of the candidate gRNAs, I selected gRNAs with 5'-GN20GG-3 and 5'-GGN19GG-3' sequences. I prepared a set of oligonucleotides for each gRNA targeted site, to integrate in the modified pDR274 vector. These included forward (5'-ATA-GN19-3' or 5'-ATA-GGN18-3') and reverse (5'-AAAC-N19-3' or 5'-AAAC-N18C-3') sequences (Table 5). Guide RNAs were synthesized using the pDR274 vector and a MEGA shortscript T7 Transcription Kit (Ambion), according to the manufacturer's instruction and previously described methods (Horch et al., 2017). A 1 μg/μl volume of gRNAs was prepared with an injection solution, and was preserved at -80 °C. The ssODN donor template was designed to contain 60 nt homologous sequences flanked by a 13 nt insertion sequence, 5'-AATAAATAGATAG-3'. These homologous sequences were directly adjacent to each Cas9-mediated DSB site in the gRNA-1 and gRNA-5 sites. The insertion sequence was designed to generate a stop codon in any reading frame. The donor template was synthesized and HPLC-purified by Eurofins Genomics (Tokyo, Japan). 2.4 μg/μl volume of the donor template was prepared with water, and was preserved at -20 °C.

Microinjection of Cas9 mRNA and gRNA

Fertilized eggs were collected with wet kitchen towels for 1-h from WT adults deprived of water for 12-h. The collected eggs were incubated at 30 °C for 1-h. Prepared Cas9 mRNA

and gRNA were mixed on ice with the injection solution and adjusted to a final concentration of 100 and 50 ng/μl, respectively, or 500 and 250 ng/μl, respectively. A 3 μl volume of the Cas9 mRNA and gRNA mixture on ice was infused in a micropipette needle. The needle was set in a micromanipulator. Incubated eggs were aligned in grooves of 1% agarose gel filled with PBS, and approximately 4 nl of the mixture was injected per egg using a microinjector (Narishige IM300 Microinjector) and compressor (Narishige 0.2LE-8SBZN), as previously described (Horch et al., 2017). Injection was performed within 4-h of collecting eggs. Injected eggs were incubated at 30 °C in 1% penicillin and streptomycin/PBS from the day of injection to the second day, and were then placed in wet kitchen towels from the third day to the hatching stage.

Microinjection of Cas9 mRNA and gRNA together with ssODNs

Fertilized eggs were collected and incubated in the same way of the microinjection of Cas9 mRNA and gRNA. Prepared Cas9 mRNA and two gRNAs were mixed on ice with the injection solution and made to a final concentration of 100 and 50 ng/μl, respectively. In parallel, ssODNs were mixed on ice with the Cas9 mRNA and gRNA to make final concentrations of 24, 240, and 2000 ng/μl. In the same way of the microinjection of Cas9 mRNA and gRNA, 3 μl of the Cas9 mRNA, gRNA, and ssODN mixtures on ice were infused in a micropipette needle. The needle was set in a micromanipulator. Incubated eggs were aligned in grooves of 1% agarose gel filled with PBS. Approximately 4 nl of the mixture was injected per egg under the control of a microinjector and compressor, as previously described (Horch et al., 2017). Injection was performed within 4-h of collecting eggs. Injected eggs were incubated in the same way of the microinjection of Cas9 mRNA and gRNA.

Genomic DNA extraction and mutation detection assay

Genome extraction was performed on eggs and legs using a Cica Geneus Total DNA Preparation Kit (Kanto Kagaku), according to the manufacturer's instructions. DNA fragments of about 200 to 300 bp in each gRNA targeted site were amplified by PCR in 20 µl reaction solution (Table 5 for used primer sequences). To form a heteroduplex containing mismatched strands, 10 µl of the PCR product was annealed following a previously described method (Watanabe et al., 2012). A 1 µl volume of Guide-it Resolvase of a Guide-it Mutation Detection Kit (Takara Bio) was added to the PCR product, and was treated at 37 °C for 15 min. The PCR products treated and untreated by the Guide-it Resolvase were applied to 3% agarose gel. Then, indel mutations in the targeted sites were detected by agarose gel electrophoresis.

Cuticle preparation

The embryos were cleaned in lactic acid at 65 °C overnight (Ronco et al., 2008). Cuticles of the embryos were mounted flat on 50% glycerol/ PBS. Digital images were taken with a Nikon DS-Ri2 digital camera connected to a Nikon SMZ18 stereomicroscope with a Nikon LED transmission dark field unit P-DF.

Embryo fixation and whole-mount in situ hybridization

Embryo fixation and whole-mount in situ hybridization with digoxigenin (DIG)-labeled antisense RNA probes were performed, as previously described (Niwa et al., 2000).

8. References

Akam, M., 1987. The molecular basis for metameric pattern in the *Drosophila* embryo. Development 101, 1-22.

Awata, H., Watanabe, T., Hamanaka, Y., Mito, T., Noji, S., Mizunami, M., 2015. Knockout crickets for the study of learning and memory: Dopamine receptor Dop1 mediates aversive but not appetitive reinforcement in crickets. Sci Rep. 5, 15885.

Chaverra-Rodriguez, D., Benetta, E.D., Heu, C.C., Rasgon, J.L., Ferree, P.M., Akbari, O.S., 2020. Germline mutagenesis of Nasonia vitripennis through ovarian delivery of CRISPR-Cas9 ribonucleoprotein. Insect Mol. Biol. 29, 569-577.

Chaverra-Rodriguez, D., Macias, V.M., Hughes, G.L., Pujhari, S., Suzuki, Y., Peterson, D.R., Kim, D., McKeand, S., Rasgon, J.L., 2018. Targeted delivery of CRISPR-Cas9 ribonucleoprotein into arthropod ovaries for heritable germline gene editing. Nat. Commun. 9, 3008.

Choe, C.P., Miller, S.C., Brown, S.J., 2006. A pair-rule gene circuit defines segments sequentially in the short-germ insect *Tribolium castaneum*. Proc. Natl. Acad. Sci. U. S. A. 103, 6560-6564.

Clark, E., 2017. Dynamic patterning by the *Drosophila* pair-rule network reconciles long-germ and short-germ segmentation. PLOS Biol. 15, e2002439.

Clark, E., Peel, A.D., Akam, M., 2019. Arthropod segmentation. Development 146, 170480.

Cong, L., Ran, F.A., Cox, D., Lin, S., Barretto, R., Habib, N., Hsu, P.D., Wu, X., Jiang, W., Marraffini, L.A., Zhang, F., 2013. Multiplex genome engineering using CRISPR/Cas systems. 339, 819-823.

Coulter, D.E., Wieschaus, E., 1988. Gene activities and segmental patterning in *Drosophila*: analysis of *odd-skipped* and pair-rule double mutants. Genes Dev. 2, 1812-1823.

Davis, G.K., Patel, N.H., 2002. Short, long, and beyond: molecular and embryological approaches to insect segmentation. Annu. Rev. Entomol. 47, 669-699.

Donoughe, S., Extavour, C.G., 2015. Embryonic development of the cricket *Gryllus bimaculatus*. Dev. Biol. 411, 140-156.

Fujioka, M., Jaynes, J.B., Goto, T., 1995. Early *even-skipped* stripes act as morphogenetic gradients at the single cell level to establish *engrailed* expression. Development 121, 4371-4382.

Fujioka, M., Yusibova, G.L., Patel, N.H., Brown, S.J., Jaynes, J.B., 2002. The repressor activity of Even-skipped is highly conserved, and is sufficient to activate *engrailed* and to regulate both the spacing and stability of parasegment boundaries. Development 129, 4411-4421.

Gao, G., McMahon, C., Chen, J., Rong, Y.S., 2008. A powerful method combining homologous recombination and site-specific recombination for targeted mutagenesis in *Drosophila.* Proc. Natl. Acad. Sci. U.S.A. 105, 13999-14004.

Hannibal, R.L., Patel, N.H., 2013. Whaat is asegment? EvoDevo 4, 35.

Heu, C.C., McCullough, F.M., Luan, J., Rasgon, J.L., 2020. CRISPR-Cas9-Based Genome Editing in the Silverleaf Whitefly (Bemisia tabaci). CRISPR J. 3, 89-96.

Horch, H.W., Mito, T., Popadić, A., Ohuchi, H., Noji, S., 2017. The cricket as a Model Organism: Development, Regeneration, and Behavior. Springer.

Huang, J., Zhou, W., Dong, W., Watson, A.M., Hong, Y., 2009. Directed, efficient, and versatile modifications of the *Drosophila* genome by genomic engineering. Proc. Natl. Acad. Sci. U.S.A. 106, 8284-8289.

Kobayashi, M., Goldstein, R.E., Fujioka, M., Paroush, Z., Jaynes, J.B., 2001. Groucho augments the repression of multiple Even skipped target genes in establishing

parasegment boundaries. Development 128, 1805-1815.

Lawrence, P.A., 1992. The Making of a Fly: The Genetics of Animal Design. Blackwell Scientific Publications, Oxford.

Lawrence, P.A., Johnston, P., 1989. Pattern formation in the *Drosophila* embryo: allocation of cells to parasegments by *even-skipped* and *fushi tarazu*. Development 105, 761-767.

Liu, P.Z., Kaufman, T.C., 2005. *even-skipped* is not a pair-rule gene but has segmental and gap-like functions in *Oncopeltus fasciatus*, an intermediate germband insect. Development 132, 2081-2092.

Macdonald, P.M., Ingham, P., Struhl, G., 1986. Isolation, structure, and expression of *even-skipped*: a second pair-rule gene of *Drosophila* containing a homeo box. Cell 47, 721-734.

Mali, P., Yang, L., Esvelt, K.M., Aach, J., Guell, M., DiCarlo, J.E., Norville, J.E., Church, G.M., 2013. RNA-guided human genome engineering via Cas9. Science. 339, 823-826.

Misof, B., Liu, S., Meusemann, K., Peters, R.S., Donath, A., Mayer, C., Frandsen, P.B., Ware, J., Flouri, T., Beutel, R.G., et al., 2014. Phylogenomics resolves the timing and pattern of insect evolution. Science 346, 763-767.

Mito, T., Kobayashi, C., Sarashina, I., Zhang, H., Shinahara, W., Miyawaki, K., Shinmyo, Y., Ohuchi, H., Noji, S., 2007. *even-skipped* has gap-like, pair-rule-like, and segmental functions in the cricket *Gryllus bimaculatus*, a basal, intermediate germ insect (Orthoptera). Dev. Biol. 303, 202-213.

Mito, T., Noji, S. 2008. The Two-Spotted Cricket *Gryllus bimaculatus*: An Emerging Model for Developmental and Regeneration Studies. C.S.H. Protoc. 2008, pdb.emo110.

Nakamura, T., Mito, T., Miyawaki, K., Ohuchi, H., Noji, S., 2008. EGFR signaling is

required for re-establishing the proximodistal axis during distal leg regeneration in the cricket *Gryllus bimaculatus* nymph. Dev. Biol. 319, 46-55.

Nakao, H., 2015. Analyses of interactions among pair-rule genes and the gap gene *Krüppel* in *Bombyx* segmentation. Dev. Biol. 405, 149-157.

Niwa, N., Inoue, Y., Nozawa, A., Saito, M., Misumi, Y., Ohuchi, H., Yoshioka, H., Noji, S., 2000. Correlation of diversity of leg morphology in *Gryllus bimaculatus* (cricket) with divergence in *dpp* expression pattern during leg development. Development 127, 4373-4381.

Nüsslein-Volhard, C., Frohnhofer, H.G., Lehmann, R., 1987. Determination of Anteroposterior Polarity in *Drosophila*. Science 238, 1675-1681.

Nüsslein-Volhard, C., Wieschaus, E., 1980. Mutations affecting segment number and polarity in *Drosophila*. Nature 287, 795.

Osakabe, Y., Watanabe, T., Sugano, S.S., Ueta, R., Ishihara, R., Shinozaki, K., Osakabe, K., 2016. Optimization of CRISPR/Cas9 genome editing to modify abiotic stress responses in plants. Sci. Rep. 6, 26685.

Ronco, M., Uda, T., Mito, T., Minelli, A., Noji, S., Klingler, M., 2008. Antenna and all gnathal appendages are similarly transformed by *homothorax* knock-down in the cricket *Gryllus bimaculatus*. Dev. Biol. 313, 80-92.

Rosenberg, M.I., Brent, A.E., Payre, F., Desplan, C., 2014. Dual mode of embryonic development is highlighted by expression and function of *Nasonia* pair-rule genes. Elife 3, e01440.

Schwentner, M., Combosch, D.J., Nelson, J.P., Giribet, G., 2017. A phylogenomic solution to the origin of insects by resolving crustacean-hexapod relationships. Curr. Biol. 27, 1818-1824.

Shirai, Y., Daimon, T., 2020. Mutations in cardinal are responsible for the red-1 and peach

eye color mutants of the red flour beetle Tribolium castaneum. Biochem. Biophys. Res. Commun. 529, 372-378.

Watanabe, T., Ochiai, H., Sakuma, T., Horch, H.W., Hamaguchi, N., Nakamura, T., Bando, T., Ohuchi, H., Yamamoto, T., Noji, S., Mito, T., 2012. Non-transgenic genome modifications in a hemimetabolous insect using zinc-finger and TAL effector nucleases. Nat. Commum. 3, 1017.

Ylla, G., Nakamura, T., Itoh, T., Kajitani, R., Toyoda, A., Tomonari, S., Bando, T., Ishimaru, Y., Watanabe, T., Fuketa, M., Matsuoka, Y., Barnett, A.A., Noji, S., Mito, T., Extavour, C.G., 2021, Insights into the genomic evolution of insects from cricket genomes. Commun. Biol. 4, 733.

Yoshimura, A., Nakata, A., Mito, T., Noji, S., 2006. The characteristics of karyotype and telomeric satellite DNA sequences in the cricket, *Gryllus bimaculatus* (Orthoptera, Gryllidae). Cytogenet. Genomic Res. 112, 329-336.

9. Acknowledgement

I greatly appreciate Prof. Taro Mito for helpful advice and great condition for research. And I also thank President Sumihare Noji, Associate Prof. Yoshiyasu Ishimaru, Dr. Sayuri Tomonari, Assistant Prof. Takahito Watanabe for helpful discussion and comments on the manuscript. This study was funded by Grants-in-Aid for Scientific Research from the Japan Society for the Promotion of Science (KAKENHI), 19K06691 awarded to YI and 17H03945 awarded to TM.